ARTICLE OPEN

Check for updates

The involvement of 5-HT was necessary for EA-mediated improvement of post-stroke depression

Bing Deng[1,3], Wenhui Di[1,3], Haoxi Long[1], Qian He[1], Zhiyuan Jiang[1], Taiyu Nan[1], Jun Gu[1], Keni Huang[1], Hongtao Li[1], Shaoyang Cui[2], Nenggui Xu[1] and Lulu Yao[1]✉

The prevalence of depression is as high as about 30% within five years after stroke, while there is still no breakthrough in the Western medical treatments for post-stroke depression (PSD) in clinical practice. The traditional acupuncture treatment has been practiced to be effective for the therapy of PSD, but its mechanism still needs to be elucidated. With a combination of methods, including behavioral testing, immunofluorescence, in vivo electrophysiological recording, mRNA sequencing, genetic modulation, and in vivo fiber recording techniques, this study showed that electroacupuncture (EA) at *Baihui* (GV20) and *Shenting* (GV24) acupoints improved the depressive-like behaviors and neuronal electrophysiological activities in PSD model mice, which was established by bilateral injection of collagenase IV into the medial prefrontal cortex (mPFC). Moreover, it was found that the EA-mediated improvement was comparable to that of fluoxetine. The mRNA sequence analysis indicated that the 5-hydroxytryptamine (5-HT) system was involved in the pathogenesis of PSD. Meanwhile, the number of 5-HT positive neurons in the dorsal raphe nucleus (DRN) and 5-HT in the mPFC was significantly decreased, and ablation of neurons in the DRN could prevent the efficacy of EA. The neuronal activity of excitatory and inhibitory neurons in mPFC can be modulated by chemogenetic activation or inhibition of the TPH2-positive neurons in the DRN projecting to the mPFC. Together, our results have provided the insight of the biological mechanism underlying acupuncture in the treatment of PSD and revealed the scientific connotation of acupuncture in both clinical and scientific value.

Translational Psychiatry (2025)15:382 ; https://doi.org/10.1038/s41398-025-03621-y

INTRODUCTION

Post-stroke depression (PSD) is one of the most common neuropsychological disorders in stroke survivors, with a prevalence as high as about 30% [1]. Individuals with PSD often experience poor quality of life and a higher risk of mortality. Until now, PSD has often been overlooked, and some patients still do not receive an appropriate diagnosis and treatment [2, 3]. Currently, PSD is treated with a variety of rehabilitation modalities, including medical and non-medical treatments, such as psychological counseling and transcranial magnetic stimulation [4, 5]. The medical treatment for PSD is dominated by selective serotonin reuptake inhibitors (SSRIs), such as fluoxetine, paroxetine, and sertraline, which account for approximately 60% to 80% of the antidepressant market share [6, 7]. However, these drugs could increase the risk of problems, including sexual dysfunction, severe insomnia, and vomiting, thus placing a greater psychological burden on the patients [8]. Importantly, these drugs are demonstrated to be effective in only one-third of patients [9]. Therefore, it is urgent to develop safer or more effective strategies for PSD treatment in clinical practice.

A narrative article on clinical guidelines has identified 11 countries with positive recommendations for acupuncture as a strategy for PSD treatment [10]. Evidence-based medicine and meta-analysis showed that acupuncture combined with antidepressants is more effective than medications alone in treating PSD [11, 12]. Meanwhile, the acupuncture treatment is well-recognized for its reliability and safety with few adverse reactions, thus it is suggested to be an ideal complementary and alternative therapy for PSD treatment [13, 14]. However, the underlying mechanism of the acupuncture treatment has still been elusive. Multiple factors have been reported to be associated with the pathologies of PSD, including the glutamatergic system, gut-brain axis, hypothalamic-pituitary-adrenal (HPA), neuroinflammation, and monoamine dysfunction [4, 5, 8]. At the neurochemical level, the most widely accepted hypothesis concerns an imbalance in the serotonin system in the brains of depressed patients [15]. The reductions in serotonin-related metabolites, including 5-HT in the cerebrospinal fluid, were related to PSD severity [16, 17]. Some studies have shown that EA could treat depression by modulating the serotonin system, such as the expression of alanine, tryptophan hydroxylase, serotonin levels, restoring synaptic plasticity, and increasing the expression of brain-derived neurotrophic factor (BDNF) [18, 19]. Thus, in this study, we aimed to investigate the involvement of 5-HT during the mechanism underlying the EA-mediated therapy of PSD.

In the study, we have established a PSD mouse model by collagenase IV injection into the medial prefrontal cortex (mPFC)

[1]South China Research Center for Acupuncture and Moxibustion, Medical College of Acu-Moxi and Rehabilitation, Guangzhou University of Chinese Medicine, Guangzhou 510006, China. [2]Shenzhen Hospital (Fu Tian) of Guangzhou University of Chinese Medicine, Shenzhen 518000, China. [3]These authors contributed equally: Bing Deng, Wenhui Di. ✉email: yaolulu@gzucm.edu.cn

Received: 25 July 2024 Revised: 11 August 2025 Accepted: 1 September 2025
Published online: 06 October 2025

and found that EA at *Baihui* (GV20) and *Shenting* (GV24) acupoints were effective in improving the depressive-like phenotypes, including the behavioral tests and electrophysiological properties, which efficacy was comparable to that fluoxetine treatment for PSD. Moreover, the results of mRNA sequence analysis suggested that the serotonin system in mPFC played a role in the pathogenesis of PSD. The expression of 5-HT in the mPFC and dorsal raphe nucleus (DRN) participated in the therapeutic effect of EA treatment against PSD, and the silencing of the function of DRN could abolish the EA-mediated effect. Furthermore, we found that both the excitatory and inhibitory neurons in the mPFC were structurally and functionally modulated by TPH2 neurons in the DRN.

MATERIALS AND METHODS

Animals

Male C57BL/6 mice (2–3 months old, 20–25 g) were purchased from the Animal Laboratory Center at Guangzhou University of Chinese Medicine. All mice were housed in one cage per 5 mice in a standard laboratory room in which the temperature was 23–25 °C, the humidity was 50–60%, and the light/dark cycle was maintained for 12 h per day (lights on from 07:00 until 19:00), with water and food available *ad libitum*. All experimental protocols were approved by the Experimental Animal Ethics Committee of Guangzhou University of Traditional Chinese Medicine (approval *No. 20230611008*) and followed the guidelines of animal bioethics. The researcher used random number assignment to randomize groups for each experiment.

PSD modeling

As described previously, the brain stereotactic injection procedure was performed, during which the mice were continuously anesthetized using isoflurane and maintained at 36.5 ~ 37.5 °C with a thermostatic heating blanket, and collagenase IV was dissolved in artificial cerebrospinal fluid (ACSF) at a concentration of 0.125 U/μl [20]. The dissolved collagenase IV was injected into the bilateral mPFC (AP: +2.0 mm, ML: ±0.5 mm, DV: −2.5 mm) with 200 nl on each side at a rate of 50 nl/min, and the needle was kept in injection site for 5 min at the end of the injection and then removed [21]. After surgery, mice were placed in a 37 °C incubator to maintain body temperature until they regained mobility. For the control group, the same injection of ACSF was administered.

Electroacupuncture treatment

Seven days after collagenase IV injection, mice were treated with EA at GV20 and GV24 for 14 consecutive days, with 15 min once a day. The GV20 and GV24 acupoints belong to the Du Meridian, and there is a close relationship between the Du Meridian and the brain. On the human, the GV20 is located directly above the tips of the two ears, right in the center of the head; GV24 is located on the head, 0.5 inches straight up from the center of the front hairline (Fig. S1) *(WHO Standard Acupuncture Point Locations in the Western Pacific Region (WHO Standard))*. Referring to the human anatomy, the GV20 in mice is located at the midpoint of the line connecting the tip of the mouse ear, where neurovascular structures are abundant (such as the occipital nerve and frontal branch), and its deep part corresponds to the brain (the motor area of the central cortex and the lateral central lobules). GV24 is located 1.3 mm directly above the midpoint of the mouse's eyes, which is located on the forehead, and the deep part corresponds to the frontal lobe [22]. Disposable acupuncture needles (0.16 × 10 mm, Suzhou Medical Appliance Factory, China) were inserted horizontally into two acupoints at a depth of 5 mm toward the tip of the nose. After insertion, the needles were connected to electrodes for continuous-wave electrical stimulation (2 Hz in frequency, and 1 mA in intensity) to the mice's heads with slight trembling [23]. For sham EA, acupuncture needles were secured to the same acupoints with tape without penetrating the skin or attaching electrodes [24]. The treatment period in the fluoxetine group was consistent with that of the EA group, with two weeks of intraperitoneal injection (5 mg/kg) [25].

Open field test (OFT). This test was widely used to detect voluntary movement and anxiety behavior in rodents. The mice were carefully placed in the center of the open field reaction box, consisting of black square plates 100 × 100 × 50 cm (L×W×H). An automatic tracking and analyzing system was used to record the movement of the mice for 5 min of free movement in the experimental box. In this assay, the index was the distance of movement in the central region of the mouse.

Forced swimming test (FST). Mice were carefully placed in transparent cylindrical buckets of water (temperature 23–25 °C; diameter 20 cm, height 27 cm) for 6 min, the depth of the water of 15 cm being such as to prevent the animals from touching the bottom with their hind limbs. Animal behavior was video-tracked from the side, and observations of how long each animal remained motionless during the test were recorded using an experiment analyzer. Immobility was defined as the absence of any active movement other than that required to prevent the animal from drowning. The animals were habituated for the first 2 min, and their behaviors were analyzed over the next 4 min. The time spent immobile during the 4 min test period was counted offline by an observer blinded to animal treatment.

Tail suspension test (TST). A 5 cm tube was attached to the tail of the mouse, taped to the tail, and suspended 50 cm above a tabletop for 6 min. Animal behavior was video-tracked from the side, and the amount of time that each animal remained stationary during the test was recorded using a tail-suspension assay analyzer. Immobility was defined as mice not struggling without any active movement. The animals were habituated for the first 2 min, and the time spent immobile during the subsequent 4 min test period was counted offline by an observer blinded to animal treatment.

Sucrose preference test (SPT). The sugar water preference test evaluates the lack of pleasure in mice. The procedure was as follows: each animal was individually housed during the 3-day testing period. On the first day, the mice were fasted for 24 h. On the second day, each mouse was given a bottle of 2% sucrose solution and a bottle of drinking water for the sugar-water test. 24 h later, the positions of the sucrose and drinking water bottles were changed once in order to prevent potential drinking position preference. After 24 h, the weights of the drinking water and sugar water before and after the test were measured to determine the intake of the mice. Sucrose preference percentage (%) = sucrose solution consumption (g) / (sucrose solution consumption (g)+ water consumption (g)) × 100%.

Immunofluorescence

Preparation of frozen sections of mouse brain: Mice were transcardially perfused with saline, followed by 4% paraformaldehyde (PFA). The brains were immersed in 4% PFA and stored in a refrigerator at 4 °C overnight. 24 h later, the brains were replaced with 15% sucrose solution, and then with 30% sucrose solution until the brains were completely immersed. The tissues were then frozen and cut into 40 μm sections with a freezing microtome (Thermo, USA). The brain slices were washed three times with PBS, each time for 10 min. Then the brain slices were incubated with 10% goat serum (Boster, AR0009) and 0.1% Triton X-100 (Biosharp, BL935A, China) in PBS for 1 h at room temperature, followed by incubation with primary antibodies at 4 °C overnight. Primary antibodies included mouse anti-NeuN (dilution 1:500, Sigma-Aldrich, Catalog No. MAB377), rabbit anti-CAMKII (dilution 1:200, Abcam, Catalog No. ab52476), rabbit anti-GABA (dilution 1:500, Sigma-Aldrich, Catalog No. A2052), and rabbit anti-5-HT (dilution 1:500, Immunostar, Catalog No. 20080).

Next, the sections were incubated with secondary antibodies at room temperature for 1 h. Secondary antibodies included IgG conjugated to Alexa Fluor 594 (goat anti-mouse, dilution 1:500, Abcam, Catalog No. ab150116), IgG conjugated to Alexa Fluor 488 (goat anti-rabbit, dilution 1:500, Thermo Fisher, Catalog No. A11034). Finally, sections were washed in PBS and incubated with 4,6-diamidino-2-phenylindole (DAPI, 1μg / 5 ml, Sigma-Aldrich, Catalog No. 28718-90-3) for staining of nuclei. The sections were imaged with a confocal microscope (Nikon) at 20× or 40× magnification. Confocal images were acquired, and cell counts were performed using ImageJ software.

Enzyme-linked immunosorbent assay

The mPFC brain region was removed on ice, stored in liquid nitrogen, and lysed by ultrasonic lysis. The protein concentration of the lysates was assessed using the BCA method to ensure consistency between the total proteins of the individual samples. The concentration of BDNF and 5-HT in serum and PFC was assayed by the ELISA kits (Jiangsu Meimian Industrial Co., Ltd., Jiangsu, China), respectively, following the vendor's prescribed methodology. Subsequently, the absorbance values were measured at 450 nm with a microplate reader.

In vivo electrophysiological recording

The mouse was anesthetized with 1.5% isoflurane (RWD, China) and placed in a stereotaxic frame for implantation with a home-made 16-channel recording electrode in the mPFC (AP: +2.0 mm; ML: ±0.5 mm; DV: −2.5 mm) and kept at 37 °C via a heating pad (RWD, China). Based on the spike width (the time interval between peak and valley), the waveforms could be classified into two types. One has a waveform width of less than 250 ms, which was defined as the characteristic of putative inhibitory neurons, and the other has a waveform width of more than 250 ms, which belongs to the putative excitatory neurons. Putative excitatory neurons with the firing rate greater than 1 Hz and less than 8 Hz, and putative inhibitory neurons with the firing rate greater than 8 Hz could be included in the statistics [26]. Spikes and LFPs were recorded for 5 min in each group by using a data acquisition system (Plexon, Dallas, TX, USA). Offline sorter v3 (Plexon, Dallas, TX, USA) was used to filter raw signals and sort spikes. Processed signals were analyzed statistically using NeuroExplorer v5 (Nex Technologies, Lexington, MA, USA). Theta (4–7 Hz) and high gamma oscillations (80–100 Hz) were extracted from the raw LFPs by using NeuroExplorer v5 (Nex Technologies, Lexington, MA, USA). The raw power spectral density was normalized to the log of PSD, which described how the power of the LFP is distributed over frequency, and was calculated using Neuroexplorer with 2048 points. After electrophysiological recordings, electrode placement was verified by sectioning the mouse brain, and data were excluded if the implantation site was not the mPFC (Fig. S4).

RNA-sequencing analysis

The mPFC biopsy specimens were collected from the control and PSD mice, and total RNA amount and integrity were assessed using the RNA Nano 6000 Assay Kit and the Bioanalyzer 2100 System (Novogene Technology Co., Ltd., Beijing, China). Transcriptome sequencing was performed at Novogene Bioinformatics Technology Co. Differential expression analysis was performed using the DESeq2 R package (1.20.0) for both sets of conditions. To control for false discovery rates, *p*-values were adjusted using the method of Benjamini and Hochberg, and the criteria for significant differential expression were set at padj < 0.05 and | log2(foldchange)| > 1, respectively.

Virus injection

Mice were anesthetized with an *i.p.* injection of avertin solution (1.25%, Sigma-Aldrich, USA) with an injection dose of 20 ml/kg, and then the scalp was incised longitudinally for approximately 1 cm to expose the skull. Two weeks before modeling, we injected rAAV-TPH2-ChR2-EGFP-WRPEs virus (200 nL with a titer of 5.49×10^{12} vg/ml; BrainVTA) into the DRN (AP: −4.6 mm; ML: +1.1 mm; DV: −3.2 mm, at a 20° angle lateral to the midline) and subsequently observed the density of the terminals in the mPFC from 5-HT neurons in the DRN for each group.

Neuronal ablation

To silence the neurons of the DRN, we injected rAAV-hsyn-taCasp3-TEVp-p2A-EGFP-WRPEs virus (200 nL with a titer of 2.72×10^{12} vg/mL; BrainVTA) in the DRN. And rAAV-hsyn-taCasp3-p2A-EGFP-WRPEs virus (200 nL with a titer of 2.60×10^{12} vg/mL; BrainVTA) was used for control [27]. Two weeks after the virus injection, molding and EA were performed. After the intervention was completed, we observed neuronal changes in the mPFC by immunofluorescence.

In vivo fiber photometry recording

We injected rAAV-hSyn-5HT3.5-WPRE-hGH pA (200 nL unilateral with a titer of 5.33×10^{12} vg/mL; BrainVTA) into the mPFC. Three weeks after injection, fiber photometry recording was carried out using a commercial device (RWD Life Science) as previously described [28]. In brief, 470- and 410-nm laser beams were first launched into the fluorescence cube and then into the optical fibers. 5-HT emission fluorescence was collected by the camera at 60fps. Once the mice were suspended in the blue box designed for TST, the in vivo recordings were carried out for 6 min. The last 4 min of TST data are included in the statistics. We calculated $\triangle F/F = (F–F1) / F0 *100\%$, where F0 was the photometry signal of the baseline (60 s after the onset of TST) and F1 was the baseline correction curve value. Only fluorescence signals of $\triangle F > 3$ s.d. were treated as events. We observed that the fluorescence signals were elevated once the mice began to struggle (**In** supplementary video). Therefore, we defined each trial as the period within 5 s after the mouse began struggling. The average of AUC values for each mouse was calculated from the fluorescence signal during the struggles of the mouse in the TST test.

Chemical genetic combined fiber photometry recording

To see if there is a functional link between mPFC and 5-HT neurons in the DRN, we combined chemogenetics and in vivo fiber photometry recording techniques. We injected rAAV-TPH2-DIO-mCherry-WPREs virus (200 nL with a titer of 5.75×10^{12} vg/ml; BrainVTA), rAAV-TPH2-DIO-hM3Dq-EGFP-WPREs virus (200 nL with a titer of 4.00×10^{12} vg/ml; BrainVTA), or rAAV-TPH2-DIO-hM4Di-mCherry-WPREs virus (200 nL with a titer of 6.22×10^{12} vg/ml; BrainVTA) in DRN. In the same mice, the rAAV-CaMKIIα-GCaMP6s-WPREs (150 nL with a titer of 5.25×10^{12} vg/ml; BrainVTA)/ rAAV-Vgat1-GCaMP6s-WPREs virus (150 nL with a titer of 5.10×10^{12} vg/ml; BrainVTA) + rAAV-retro-cre-WPREs virus (150 nL with a titer of 5.40×10^{12} vg/ml; BrainVTA) was injected into the mPFC and the optical fiber was implanted into the mPFC to observe the change of Ca^{2+} signaling of excitatory or inhibitory neurons with activation or inhibition of the TPH2-positive neurons in the DRN projecting to the mPFC.

Two weeks after viral injection, PSD modeling was initiated. Intervention begins one week after molding, the PSD+hM3Dq+CNO group was injected with clozapine N-oxide (CNO) intraperitoneally (1 mg/kg), and the PSD+hM4Di+CNO+EA group was started with EA at 30 min after CNO injection (1 mg/kg, *i.p.*). The time is consistent with the PSD+DIO+EA group. Fluorescence signals of CaMKIIα and Vgat1 were activated by excitation beams of 470 nm. Changes in fluorescence values ($\triangle F/F$) were calculated as (F-F1)/F0*100%.

Statistical analysis

To ensure impartiality, data analysis was performed in a blinded manner, and the analysts were not aware of the allocation of experimental groups. The sample size of the experiment was calculated based on our previous studies, such as behavioral testing. The sample size and specific statistical tests for each group were provided in the corresponding legends. All data are reported as mean ± SEM, Shapiro–Wilk test was used to evaluate the distribution of the data. Normally distributed data were analyzed using an independent sample t-test and one-way ANOVA with Bonferroni post hoc test, while Mann-Whitney test and Kruskal–Wallis test were used in the contrast. Data that did not exhibit a normal distribution were analyzed via a non-parametric equivalent. SPSS 22.0 was used to assess the distribution of the data, and GraphPad Prism 8 was used to perform the statistical graphing. A value of $p < 0.05$ was considered statistically significant for analysis.

RESULTS

EA improved the depressive-like phenotypes in PSD mice induced by collagenase IV injection into the bilateral mPFC

To establish the PSD mouse model, we injected the collagenase IV (0.125 U/μl) into the bilateral mPFC (AP: +2.0 mm; ML: ±0.5 mm; DV: −2.5 mm), and the ACSF was used as control [21, 29]. The combined selection of the GV20 and GV24 acupoints is one of the most frequently used acupoint groups in clinical applications for the treatment of PSD [11, 30, 31]. EA (2 Hz, 15 min) at GV20 and GV24 was administered post-injection for 7 days, with 14 consecutive days (Fig. S1). On the day after EA treatment, the depressive-like behavioral tests were examined within 7 days, and once finished, these mice were sacrificed for further analysis (Fig. 1A). The pathology of stroke was characterized by immunostaining showing that an obvious lost of mPFC tissues and neurons could be significantly reversed by EA treatment (Fig. 1B, C). To determine the neuronal type in mPFC, we have stained for the protein, including CaMKII and GABA, which are widely used as markers of the excitatory and inhibitory neurons, respectively [32]. We found that the expression of CaMKII-positive excitatory neurons was significantly reduced in the PSD mice and rescued by the EA treatment (Fig. 1D). While the expression of GABA-positive inhibitory neurons showed an increase in the PSD mice, and a comparable level in the PSD+sham-EA mice (Fig. 1E). The depressive-related phenotypes were evaluated by behavioral tests, including the open field test (OFT), force swimming test (FST), tail suspension test (TST), sucrose preference test (SPT), and BDNF assessments as well. The OFT

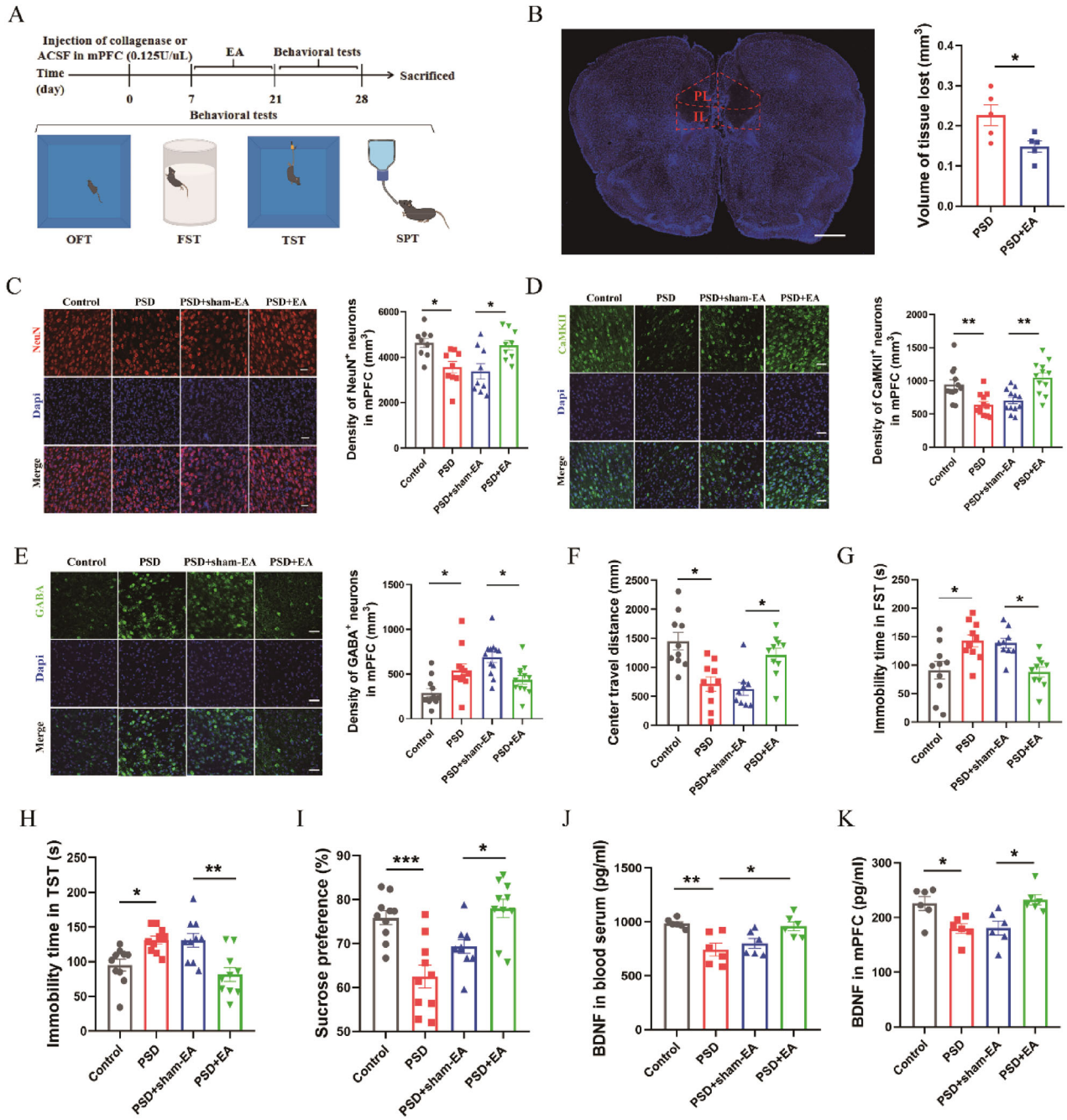

Fig. 1 EA at GV20 and GV24 improved the depression-related symptoms of PSD mice induced by collagenase IV injection at the bilateral mPFC. A The time axis of the experimental procedure and behavioral analysis among groups. **B** Left: Schematic diagram of immunofluorescence staining of mPFC tissue after 21 days of collagenase IV injection. Right: The statistical analysis of volume of tissue loss in the mPFC. (Two-tailed Student's unpaired *t* test, $N = 5$ per group). Scale bar, 500 μm. **C–E** Representative images and data statistics of immunofluorescent staining of NeuN$^+$ (red), CaMKII$^+$ (green), and GABA$^+$ (green) in the mPFC in mice of Control, PSD, PSD+sham-EA, and PSD+EA groups. (one-way ANOVA test, $N = 9$–12 slices per group). Scale bar, 50 μm. **F–I** Performance in Control or PSD mice, or PSD mice treated with sham-EA or EA for 2 weeks in OFT (F) (Kruskal-Wallis test, $N = 9$–10 per group), FST (G), TST (H), and SPT (I) (one-way ANOVA test, $N = 9$–10 per group). **J, K** Concentration of BDNF in blood serum (J) and mPFC tissue (K) was determined by ELISA kit. (one-way ANOVA test, $N = 6$ per group). Data are presented as mean ± SEM. *P* values are set to $^*P < 0.05$, $^{**}P < 0.01$, $^{***}P < 0.001$.

experiment demonstrated that there was no significant difference in the total distance traveled by PSD mice compared to the control group, indicating that motor function was not affected in PSD mice (Fig. S2). However, the central travel distance was reduced, and this symptom was improved by EA (Fig. 1F). In addition, the results obtained by FST and TST demonstrated that the immobility time was increased in the PSD mice or the PSD mice with sham-EA compared to that in the control mice, and these increased immobility time were relieved after EA treatment (Fig. 1G, H). Moreover, PSD mice or PSD mice with sham-EA showed less preference for sucrose in SPT, and EA could alleviate this hypofunction (Fig. 1I). Furthermore, the concentration of BDNF in both serum and mPFC tissues measured by ELISA was reduced in PSD mice, which could be reversed by EA (Fig. 1J, K). It is worth mentioning that we have also attempted to inject collagenase IV in the left mPFC (AP: +2.0 mm; ML: +0.5 mm; DV: −2.5 mm), while the

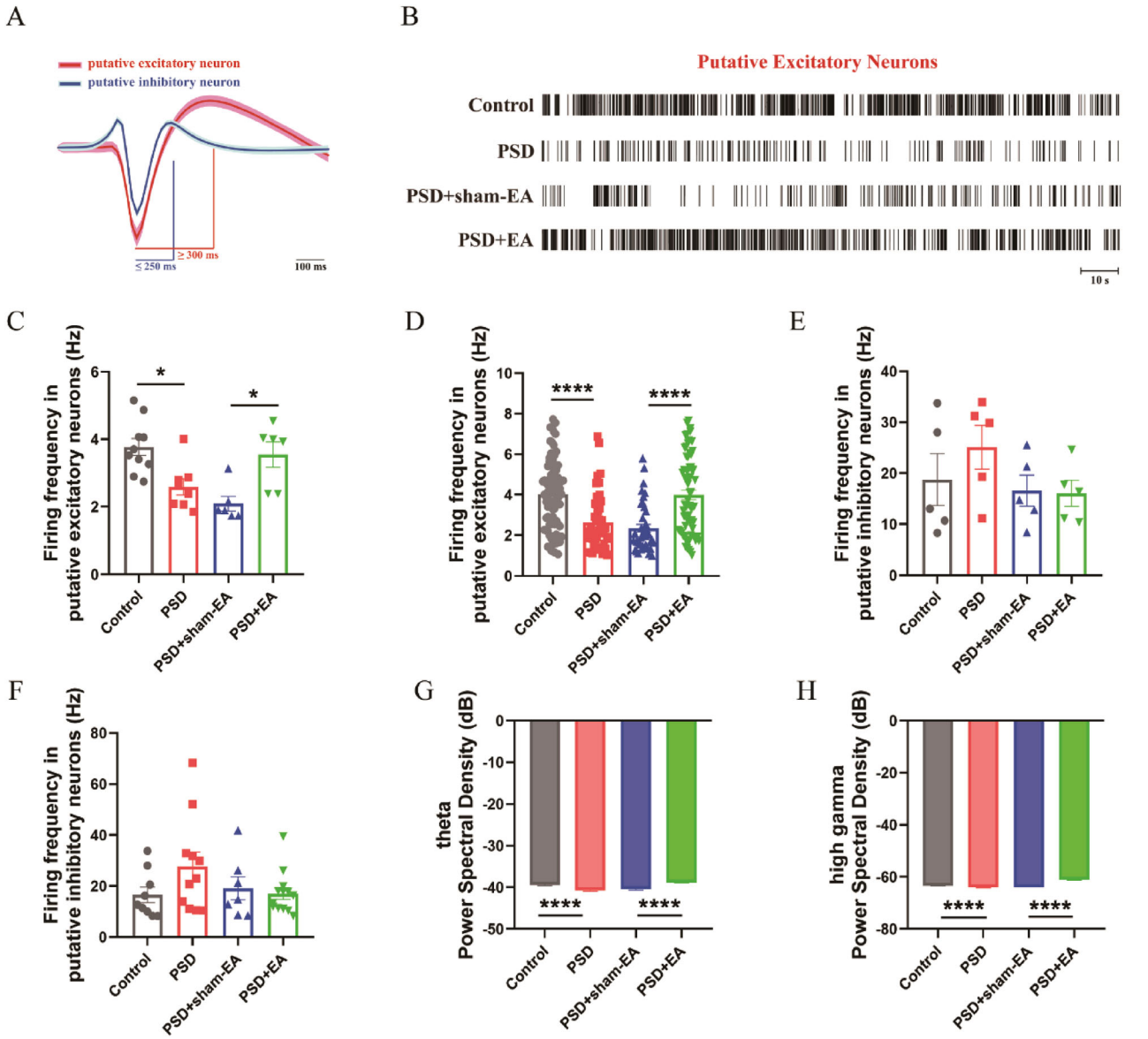

Fig. 2 EA modulated the neuronal electrophysiological activity in the mPFC of PSD mice. A Samples for waveforms of putative excitatory neurons and putative inhibitory neurons. Scale bar, 100 ms. **B** Representative rasters of spikes from putative excitatory neurons. Scale bar, 10 s. **C** The statistical analysis of the firing frequency of the putative excitatory neurons for each mouse. (one-way ANOVA test, $N = 6–10$ per group). **D** The statistical analysis of the firing frequency of the putative excitatory neurons for each unit. (Kruskal-Wallis test, $N = 234$ units). **E** The statistical analysis of the firing frequency of the putative inhibitory neurons for each mouse (one-way ANOVA test, $N = 5$ per group). **F** The statistical analysis of the firing frequency of the putative inhibitory neurons for each unit (Kruskal-Wallis test, $N = 40$ units). **G** The statistical analysis of power spectrum results in theta oscillation from the mPFC neurons (Kruskal-Wallis test, $N = 5$ per group). **H** The statistical analysis of power spectrum results in high gamma rhythms from the mPFC neurons (Kruskal-Wallis test, $N = 5$ per group). Data are presented as mean ± SEM. P values are set to $^{*}P < 0.05$, $^{****}P < 0.0001$.

results showed that there were no significant depressive-like phenotypes in mice (Fig. S3A–D).

Altogether, these results suggested that the PSD mouse model induced by injecting collagenase IV into the bilateral mPFC was characterized by loss of tissues or neurons in mPFC, depressive-like behaviors, a reduced expression of CaMKII-positive excitatory neurons with an increase of GABA-positive inhibitory neurons, and an attenuated level of BDNF. Meanwhile, EA at GV20 and GV24 acupoints could improve these pathologies.

EA modulated the impairments of neuronal activity in the mPFC of PSD mice in vivo

It has been suggested that the neuronal activity in the mPFC is important in the mental state, emotion regulation ability, and homeostasis of the central nervous system, and that dysregulation or imbalance of excitatory and inhibitory neuronal activity contributes to the pathophysiology of depression [33, 34]. To directly examine the neuronal activity of pyramidal and inhibitory neurons in vivo, we implanted 16-channel electrodes into the mPFC and recorded the spontaneous firing in neurons of mice with free movement (Figs. S4, 2A). We found that the frequency of spike firing in the putative excitatory neurons of PSD mice was reduced compared with that in the control group, and EA could enhance this impairment (Fig. 2B–D). By contrast, there was no difference in the spike firing of putative inhibitory neurons among these groups, including the Control, PSD, PSD+sham-EA, and PSD+EA (Figs. S5, 2E, F). Meanwhile, local field potentials (LFPs), reflecting the regular activities of neuronal clusters and generated

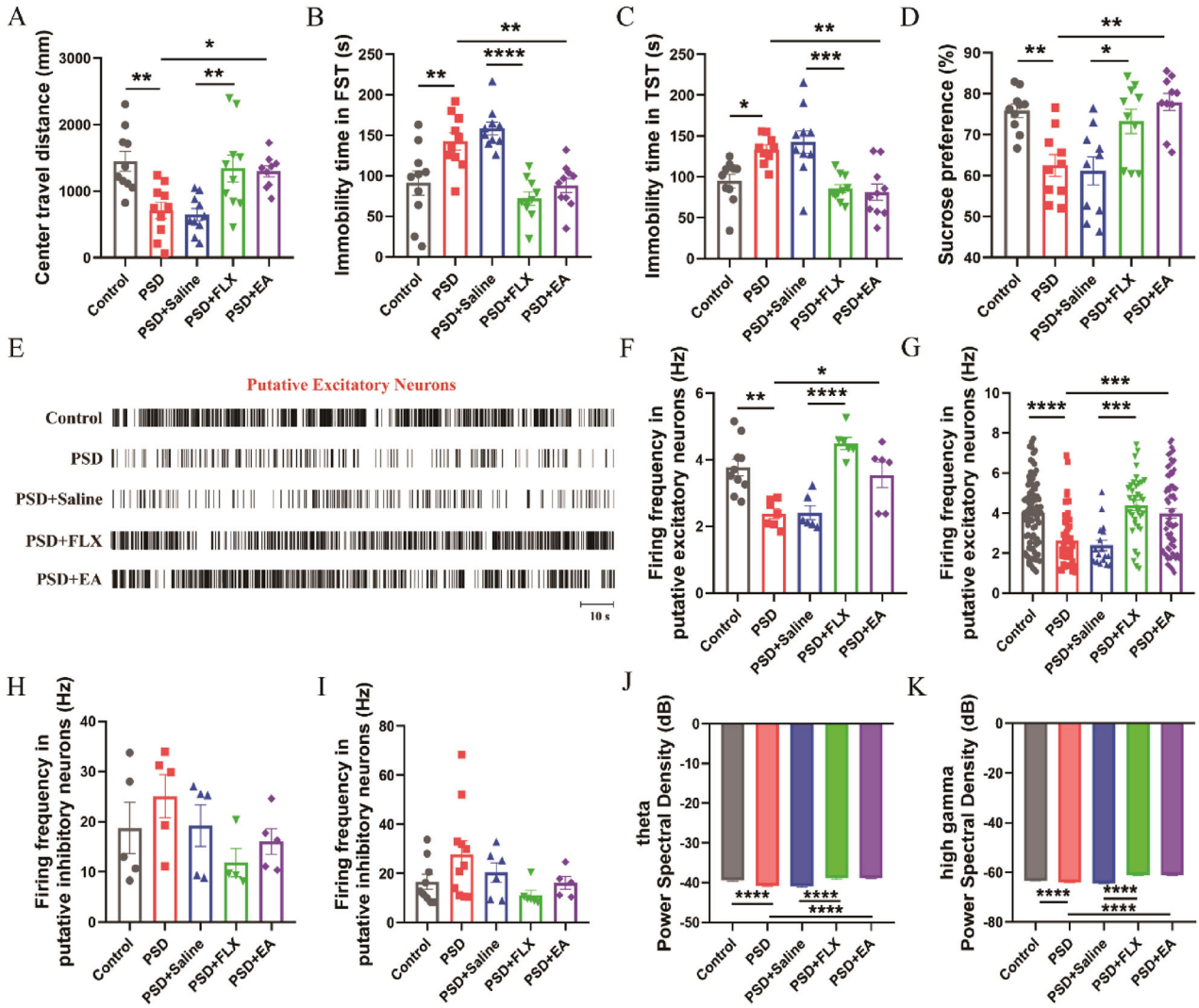

Fig. 3 EA-mediated improvement of PSD was comparable to that of fluoxetine. A–D Behavioral effects of PSD mice treated with FLX for two weeks in OFT (A), FST (B), TST (C), and SPT (D). (one-way ANOVA test, $N = 9$–10 per group). **E** Representative rasters of spikes from putative excitatory neurons. Scale bar, 10 s. **F** The statistical analysis of the firing frequency of the putative excitatory neurons for each mouse. (one-way ANOVA test, $N = 6$–10 per group). **G** The statistical analysis of the firing frequency of the putative excitatory neurons for each unit. (Kruskal-Wallis test, $N = 247$ units). **H** The statistical analysis of the firing frequency of the putative inhibitory neurons for each mouse (one-way ANOVA test, $N = 5$ per group). **I** The statistical analysis of the firing frequency of the putative inhibitory neurons for each unit (Kruskal-Wallis test, $N = 37$ units). **J** The statistical analysis of power spectrum results in theta rhythms from the mPFC neurons (Kruskal-Wallis test, $N = 5$ per group). **K** The statistical analysis of power spectrum results in high gamma rhythms from the mPFC neurons (Kruskal-Wallis test, $N = 5$ per group). Data are presented as mean ± SEM. P values are set to $^{*}P < 0.05$, $^{**}P < 0.01$, $^{***}P < 0.001$, $^{****}P < 0.0001$.

neural oscillations at different frequencies, including theta (4–7 Hz) and high gamma (80–100 Hz), have also been observed [35–37]. The results showed that the power spectral density of both theta oscillation and high gamma oscillation was significantly mitigated in the PSD, and EA relieved this attenuation (Fig. 2G, H, S6A, B). These results obtained from in vivo electrophysiological recording together suggested that the neuronal activity was dampened in the PSD mice with an impairment of excitation, which could be modulated by EA treatment.

EA-mediated improvement of PSD was comparable to that of fluoxetine and involved with the 5-HT in the mPFC

It is well-known that fluoxetine (FLX), a selective serotonin reuptake inhibitor, has been widely used to treat PSD in clinical practice, although it has some obvious side effects [17]. In this case, we aimed to compare the effects mediated by EA and FLX and unravel their underlying mechanism to promote the application of acupuncture treatment in clinical practice. In the behavioral tests, the OFT, FST, TST, and SPT have demonstrated that FLX showed great efficacy in the center travel distance, immobility time, and sucrose preference, compared to that in the saline group (Fig. 3A–D). Interestingly, the EA-mediated improvement of these behavioral phenotypes was comparable to that of FLX. In addition, spike firing obtained by in vivo electrophysiological recording showed similar results (Figs. 3E–I, S7A, B), as well as the theta and high gamma oscillation (Fig. 3J, K, S8A, B). Altogether, these results suggested that the EA-mediated improvement was comparable to the effect of fluoxetine on PSD.

Next, considering the importance of 5-HT in the pathogenesis of depression, we hypothesized that 5-HT might be involved in this EA-mediated effect. Hence, we first performed gene expression profiling in the mPFC tissue. Out of a total of 1923 differentially expressed genes (DEGs), 1607 gene transcripts exhibited upregulation, whereas 316 gene transcripts demonstrated downregulation in the PSD group relative to the control group (Fig. 4A). Performing GO analysis based on the differential genes, we

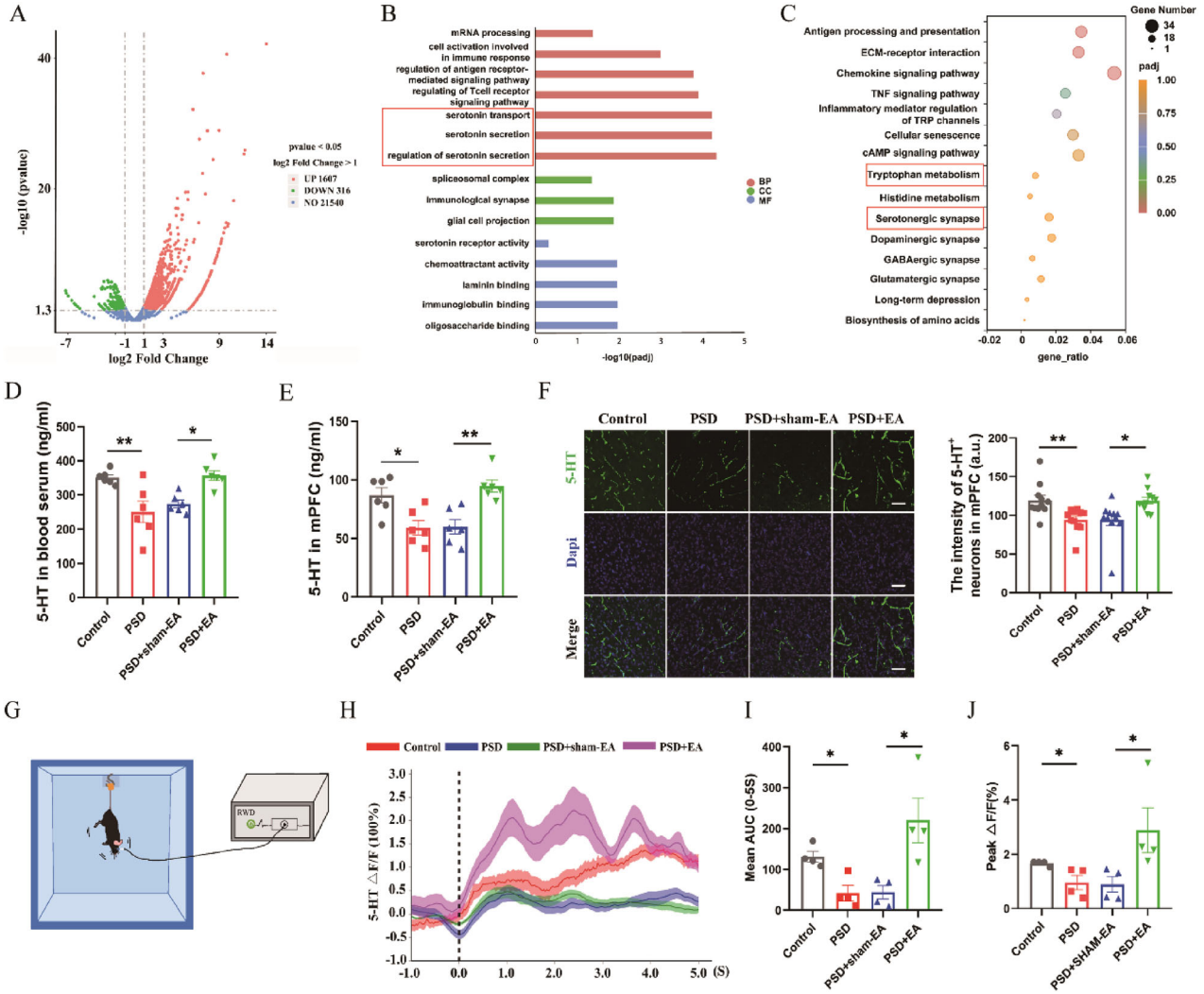

Fig. 4 EA relieved the impairment of 5-HT expression/function in the mPFC in the PSD. A A volcano plot was constructed to visualize the differential regulation of gene expression between the Control and PSD groups, as determined by RNA-Seq analysis. These upregulated and downregulated genes were demonstrated in red and green. **B** Gene Ontology (GO) functional analysis shows enriched items in the ranked PSD-related DEGs. BP, biological process; CC, cellular component; MF, molecular function. **C** The Kyoto Encyclopedia of Genes and Genomes (KEGG) analysis pathway enrichment analysis was performed to evaluate the targets linked to PSD ChIP-seq peaks. **D, E** 5-HT content in blood serum (D) and the mPFC (E) was determined by ELISA kit. EA significantly increased the expression level of 5-HT in the PSD mice. (one-way ANOVA test, $N = 6$ per group). **F** Left: Representative images of immunofluorescent staining of 5-HT (green) in the mPFC from Control, PSD, PSD+sham-EA, and PSD+EA groups. Right: The intensity of 5-HT was significantly reduced by PSD induction, and this impairment could be recovered by EA treatment. (one-way ANOVA test, $N = 11$ slices per group). Scale bar, 50 μm. **G** Illustration showing TST and in vivo fiber photometry recording. **H** Line plots showing changes in 5-HT signal activation between the four groups during the struggle of mice in TST. **I** The statistical analysis of the mean area under the curve (AUC) of 5-HT activity during the struggle phase of mice in TST. (Mann-Whitney test, $N = 4$ per group). **J** The statistical analysis of peak ΔF/F in TST. (Mann-Whitney test, $N = 4$ per group). Data are presented as mean ± SEM. P values are set to $^{*}P < 0.05$, $^{**}P < 0.01$.

identified several serotonin-related functions, including regulation of serotonin secretion, serotonin secretion, serotonin transport, and serotonin receptor activity (Fig. 4B). In KEGG pathway analysis, it was indicated the pathology of PSD might be correlated with serotonergic systems, such as tryptophan metabolism and serotonergic synapse (Fig. 4C). Overall, the RNA sequence analysis has referred to the role of 5-HT in the pathogenesis of PSD. The result was further confirmed by ELISA analysis and immunofluorescence staining showing that the concentration of 5-HT in both the mPFC and serum was reduced, as well as the density of 5-HT expression in the mPFC, and all of these impairments were ameliorated by EA (Fig. 4D–F).

Based on the above in vitro experiments, we found that the 5-HT system played an important role in PSD and EA-mediated effects. To further directly investigate the role of 5-HT in the PSD or EA-mediated effect in vivo, we recorded the signaling levels of 5-HT using fiber photometry (Fig. 4G). A virus of AAV-hSyn-5HT3.5 was injected into the mPFC, followed by fiber implantation. The response of 5-HT was measured by observing the changes in fluorescence signals during TST, which could reflect the function of the 5-HT transmitter in response to the depressive executions [38, 39]. It was found that the fluorescence signals were elevated once the mice began to struggle. The response of 5-HT signals during the struggle was decreased in the PSD mice, while this deficit was recovered by the intervention of EA (Fig. 4H–J). In summary, both in vitro and in vivo results indicated that 5-HT function was mitigated in PSD and that EA could improve this impairment.

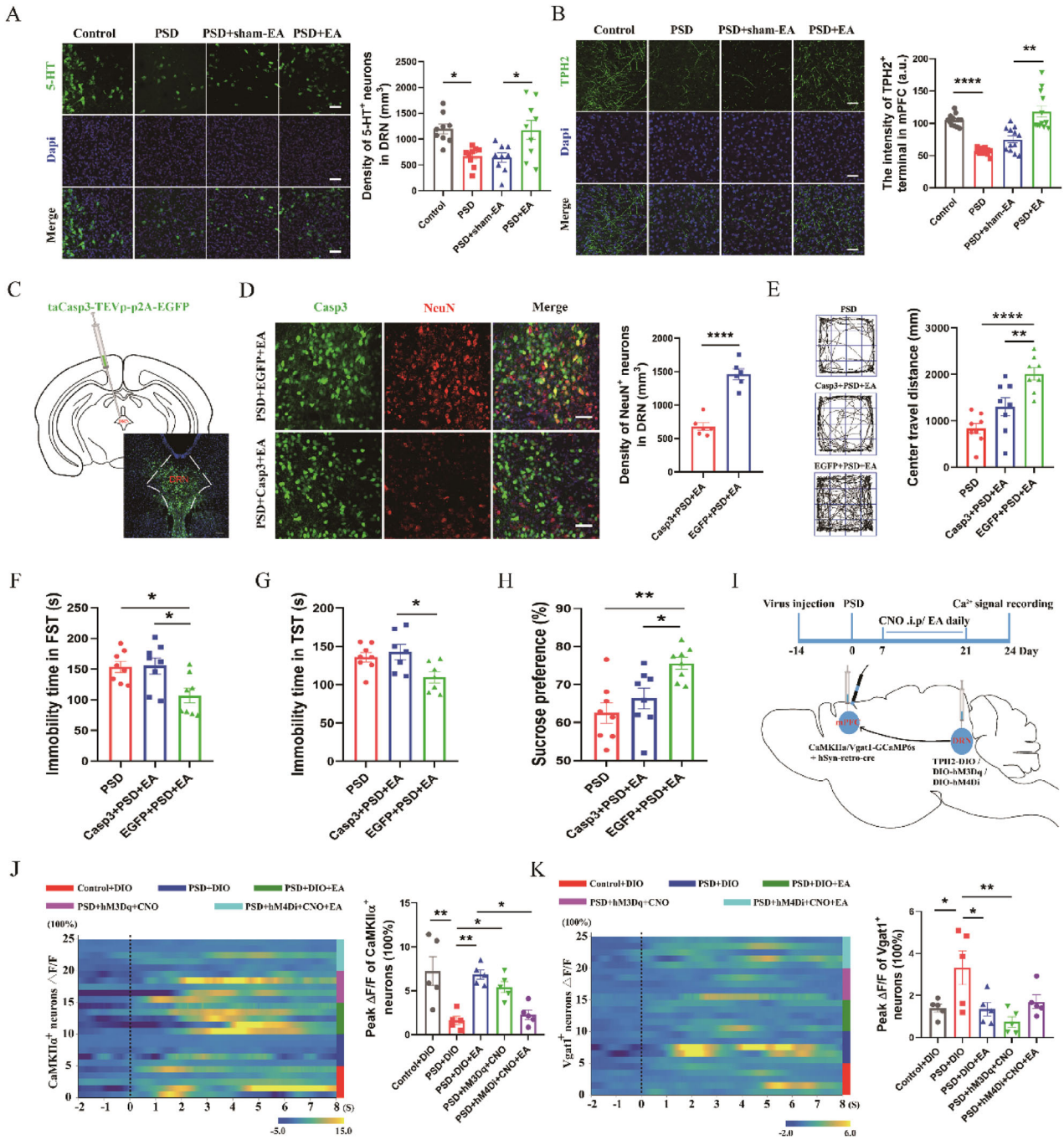

The EA-mediated effect on PSD was dependent on the function of DRN

The vast majority of 5-HT neurotransmitters in the central nervous system are derived from neurons in the DRN brain region, which axon terminals projected to the mPFC, VTA (ventral tegmental area), BNST (the bed nucleus of the stria terminals) and released the 5-HT, we speculated that the expression of 5-HT in mPFC might be due to the pathology of DRN [40, 41]. Thus, immunofluorescence staining of 5-HT neurons in the DRN was first examined. The results showed that the density of 5-HT in the DRN was obviously attenuated in the PSD or PSD with sham-EA mice, and EA treatment showed a restoration (Fig. 5A).

To further ascertain the role of DRN during the EA-mediated improvement of PSD, we have injected rAAV-TPH2-ChR2-EGFP-WRPEs virus, which are widely used to label the 5-HT-positive neurons with EGFP [42], into the DRN. The EGFP-positive terminals in the mPFC were observed, indicating there was a structural connection from 5-HT neurons in the DRN to the neurons in the mPFC (Fig. S9A). The results showed that the density of the terminals in the mPFC from 5-HT neurons in the DRN was significantly reduced in the PSD mice, compared to the control group, and this abnormality was repaired by EA (Fig. 5B). Subsequently, we downregulated the function of neurons in DRN by injecting the rAAV-hsyn-taCasp3-TEVp-p2AEGFP-WRPEs virus, which was widely used to ablate the neurons in the infected regions, and rAAV-hsyn-taCasp3-p2A-EGFP-WRPEs as a control virus (Fig. 5C) [43]. The results showed a significant loss of neurons in the Casp3+PSD+EA group compared to the EGFP+PSD+EA group, which confirmed the efficacy of the virus transfection (Fig. 5D). Furthermore, the effect of EA on the increase of center travel

Fig. 5 The involvement of 5-HT was required in the EA-mediated effect on PSD. A Left: Representative images of immunofluorescent staining of 5-HT$^+$ neurons (green) in the DRN from Control, PSD, PSD+sham-EA, and PSD+EA groups. Right: The graphical plot of the density of 5-HT. (one-way ANOVA test, $N = 9$ per group). Scale bar, 50 μm. **B** Left: Confocal images showing TPH2$^+$ fibers in mPFC from DRN. Right: The intensity of TPH2$^+$ terminal in mPFC from DRN was significantly reduced by PSD induction, and this impairment could be recovered by EA treatment. (Kruskal-Wallis test, $N = 12$ slices per group). Scale bar, 50 μm. **C** Diagram of rAAV-hsyn-taCasp3-TEVp-p2A-EGFP-WRPEs or rAAV-hsyn-taCasp3-p2A-EGFP-WRPEs virus was injected into DRN (green); blue, DAPI. Scale bar, 100 μm. **D** Left: The number of NeuN$^+$ neurons was ablated significantly in the Casp3+PSD+EA group compared with the EGFP+PSD+EA group. Right: The density of NeuN$^+$ neurons was measured within the infected area. (one-way ANOVA test, $N = 11$ slices per group). Scale bar, 50 μm. **E–H** Behavioral effects of PSD mice after virus-mediated ablation of DRN neurons in OFT (E), FST (F), TST (G), and SPT (H). **I** The timeline shown upper demonstrates the experimental procedure. Schematic diagram showing the strategy used to determine whether the calcium signaling in CaMKIIα or Vgat1 neurons in mPFC was modulated by chemogenetic activation or inhibition of TPH2-positive neurons in the DRN. rAAV-CaMKIIα-GCaMP6s/rAAV-Vgat1-GCaMP6s+rAAV-retro-cre virus was injected into the mPFC, rAAV-TPH2-DIO-mCherry, rAAV-TPH2-DIO-hM3Dq-EGFP or rAAV-TPH2-DIO-hM4Di-mCherry virus was injected into the DRN. **J** Left: Representative heatmaps illustrating the Ca^{2+} signal changes of CaMKIIα$^+$ neurons in the mPFC from the following groups: the Control group (Control+DIO, injection of rAAV-TPH2-DIO-mCherry control virus into the DRN, and injection of rAAV-CaMKIIα-GCaMP6s+rAAV-retro-cre virus into the mPFC), the PSD group (PSD+DIO, injection of rAAV-TPH2-DIO-mCherry control virus into the DRN, and injection of rAAV-CaMKIIα-GCaMP6s+rAAV-retro-cre virus into the mPFC), the PSD with EA treatment group (PSD+DIO+EA, injection of rAAV-TPH2-DIO-mCherry control virus into the DRN, injection of rAAV-CaMKIIα-GCaMP6s+rAAV-retro-cre virus into the mPFC, and treated with EA), the PSD with activation of the TPH2-positive neurons group (PSD+hM3Dq+CNO, injection of rAAV-TPH2-DIO-hM3Dq-EGFP activation virus into the DRN, injection of rAAV-CaMKIIα-GCaMP6s+rAAV-retro-cre virus into the mPFC, and CNO intraperitoneal injection), the PSD with EA after inhibition of TPH2-positive neurons group (PSD+hM4Di+CNO+EA, injection of rAAV-TPH2-DIO-hM4Di-mCherry inhibition virus into the DRN, injection of rAAV-CaMKIIα-GCaMP6s+rAAV-retro-cre virus into the mPFC, and treated with EA after CNO intraperitoneal injection). Right: The statistical analysis of peak △F/F. The Ca^{2+} signaling in excitatory neurons was increased in both the PSD+DIO+EA and the PSD+hM3Dq+CNO group compared to the PSD+DIO group. After inhibiting the TPH2-positive neurons in the PSD+hM4Di+CNO+EA group, the effect of EA on the increase of calcium signaling in CaMKIIα$^+$ neurons in the mPFC could be blocked. **K** Left: Representative heatmaps illustrating the Ca^{2+} signal changes of Vgat1$^+$ neurons in mPFC from the following groups: the Control group (Control+DIO, injection of rAAV-TPH2-DIO-mCherry control virus into the DRN, and injection of rAAV-Vgat1-GCaMP6s+rAAV-retro-cre virus into the mPFC), the PSD group (PSD+DIO, injection of rAAV-TPH2-DIO-mCherry control virus into the DRN, and injection of rAAV-Vgat1-GCaMP6s+rAAV-retro-cre virus into the mPFC), the PSD with EA treatment group (PSD+DIO+EA, injection of rAAV-TPH2-DIO-mCherry control virus into the DRN, injection of rAAV-Vgat1-GCaMP6s+rAAV-retro-cre virus into the mPFC, and treated with EA), the PSD with activation of the TPH2-positive neurons group (PSD+hM3Dq+CNO, injection of rAAV-TPH2-DIO-hM3Dq-EGFP activation virus into the DRN, injection of rAAV-Vgat1-GCaMP6s+rAAV-retro-cre virus into the mPFC, and CNO intraperitoneal injection), the PSD with EA after inhibition of TPH2-positive neurons group (PSD+hM4Di+CNO+EA, injection of rAAV-TPH2-DIO-hM4Di-mCherry inhibition virus into the DRN, injection of rAAV-Vgat1-GCaMP6s+rAAV-retro-cre virus into the mPFC, and treated with EA after CNO intraperitoneal injection). Right: The statistical analysis of peak △F/F. In the inhibitory neurons, the Ca^{2+} signaling showed a significant increase in the PSD + DIO group compared to the Control+DIO group. However, the PSD+DIO+EA group and activation of the TPH2-positive neurons in the PSD+hM3Dq+CNO group can attenuate this increased Vgat1$^+$ neuronal activity. Data are presented as mean ± SEM. P values are set to $^*P < 0.05$, $^{**}P < 0.01$, $^{****}P < 0.0001$.

distance in the OFT, the attenuation of immobility time in the FST or TST, and the enhancement of sucrose preference, were all absent after ablation of neurons in DRN (Fig. 5E–H). These results suggested that EA-mediated recovery was seriously compromised in the Cap3+PSD+EA group, compared to the EGFP+PSD+EA group.

To explore functional connectivity, we combined chemogenetics and in vivo fiber photometry recording techniques. rAAV-TPH2-DIO-mCherry, rAAV-TPH2-DIO-hM3Dq-EGFP, or rAAV-TPH2-DIO-hM4Di-mCherry virus was injected into the DRN, while rAAV-retro-cre virus was injected into the mPFC to specifically activate or inhibit the TPH2-positive neurons in the DRN projecting to the mPFC through intraperitoneal injection of CNO. In the same mice, rAAV-CaMKIIα-GCaMP6s or rAAV-Vgat1-GCaMP6s was injected into the mPFC, and the optical fiber was implanted into the mPFC to observe the change of Ca^{2+} signaling of excitatory or inhibitory neurons with activation or inhibition of the TPH2-positive neurons in the DRN projecting to the neurons in the mPFC (Fig. 5I).

We found that the Ca^{2+} signaling in excitatory neurons was increased in both the PSD mice with EA treatment and the PSD mice with activation of the TPH2-positive neurons compared to the PSD mice. After inhibiting the TPH2-positive neurons in the DRN projecting to the mPFC in the PSD mice, the effect of EA on the increase of calcium signaling in CaMKIIα-positive neurons in the mPFC was blocked (Figs. 5J, S9B). Nevertheless, in the inhibitory neurons, the Ca^{2+} signaling showed a significant increase in the PSD mice compared to the control mice. However, EA treatment or activation of the TPH2-positive neurons can attenuate this increased Vgat1 neuronal activity in the PSD mice (Figs. 5K, S9C). This suggested that the calcium signaling of the CaMKIIα- or Vgat1-positive neurons in mPFC can be modulated by chemogenetic activation or inhibition of TPH2 neurons projecting from the DRN.

Altogether, these results demonstrated the importance of 5-HT-positive neurons in the DRN projecting to the mPFC and further established the essential role of 5-HT during the EA interventions of PSD.

DISCUSSION

In this study, we established a PSD mouse model by injecting collagenase IV into the bilateral mPFC in mice, with the depressive-like phenotypes persisting for at least 28 days. We further found that both EA could improve the PSD comparable to that of FLX, and significantly restored the expression of 5-HT both in the mPFC and DRN induced by PSD. All these EA-mediated improvements of PSD were prevented after ablation of DRN neurons. Meanwhile, the calcium signaling in CaMKIIα or GABA neurons in the mPFC was structurally and functionally modulated by TPH2 neurons in the DRN. These new findings have far implications for understanding the contributions of 5-HT to the pathology of PSD and EA-mediated therapy.

Considering that intracerebral hemorrhage (ICH) is one of the deadliest types of stroke, with high rates of morbidity, mortality, and disability [1, 44–46]. Among them, survivors of ICH have a significantly high risk of PSD, with reported occurrence rates as high as 60% [47]. Furthermore, in terms of clinical treatment, selective serotonin reuptake inhibitors (SSRIs) are generally considered first-line treatment agents for PSD. While these drugs are reported to be associated with increased risk of first-ever ICH, most likely owing to their antithrombotic effects [48–50]. Last but not least, most studies on PSD have focused on ischemic stroke, and little is known about the mechanisms that lead to PSD after

hemorrhagic damage in animals. Therefore, it is necessary to establish a model of hemorrhagic stroke-induced depression, investigate the underlying mechanism, and identify more effective treatments.

Middle cerebral artery occlusion surgery combined with chronic mild stress or unpredictable chronic mild stress is the most commonly used modality for modeling PSD [51, 52]. However, the model mice with MCAO are characterized by variable lesions of the cortex and striatum, showing the obvious sensorimotor impairment that interferes with the assessment of depressive-like behavioral tests [53]. It has been shown that the probability of depression is significantly increased if the lesion location is in the mPFC and does not affect multimotor functioning [54–56]. For example, the injection of ET-1 into the mPFC creates a consistently reliable depressive model of post-ischemic stroke with no effect on motor activity or sensorimotor functions [21]. It has been suggested that the manifestations of PSD in humans are associated with lesions located in the mPFC. The clinical reports indicated that up to 70% of patients with frontal lobe hemorrhage develop depression [57, 58]. The two most widely used models of hemorrhagic stroke in laboratory studies are the collagenase model and the autologous blood injection model [59, 60]. The collagenase model is simple and highly reproducible. The injection of collagenase causes in situ rupture of blood vessels and subsequent expansion, which to some extent better simulates the pathophysiology of secondary cell death and edema caused by hematoma after ICH in humans compared to the autologous blood model [61]. Therefore, in this study, the mPFC was used as a stroke target, and a simple and reproducible model of hemorrhagic PSD was formed by disrupting the basal lamina of the cerebral blood vessels through the injection of collagenase IV, which resulted in the leakage of blood into the surrounding brain tissue [21, 62].

In addition to the mPFC injury itself, the mPFC neurons are densely innervated by 5-HT neurons originating from the DRN, which is a main source of 5-HT in the brain [63, 64]. A large number of reports have shown that there is a mutual projection relationship between mPFC and DRN [65]. Thus, it would be likely that bleeding injury in the mPFC may lead to functional impairments of DRN, and functional damage of DRN will further in turn weaken the activity of neurons in the mPFC brain region, and this interaction aggravates the occurrence of depressive-like behavior. In this study, we observed 5-HT-positive neuron terminals in the mPFC after injecting a labeling virus of 5-HT-positive neurons in the DRN, suggesting that there was a structural connection between 5-HT neurons in the DRN and neurons in the mPFC. The terminals in the mPFC from 5-HT neurons in the DRN were affected in PSD mice, and EA can repair this projection abnormality (Figs. S9A, 5B). The CaMKIIα- or Vgat1-positive neurons in mPFC were changed in the PSD and rescued by EA treatment; meanwhile, the calcium signaling can be modulated by chemogenetic activation or inhibition of the TPH2-positive neurons in the DRN projecting to mPFC (Fig. 5J, K, S9B, C).

Our findings revealed that EA at GV20 and GV24 acupoints could improve the depressive-like behaviors in the PSD model mice. Phenotypically speaking, this traditional treatment-mediated effect was found to be comparable to the FLX. In terms of mechanism, both EA and FLX treatment showed a rescue of impairment of pyramidal neuronal activity and theta- or gamma-oscillation in the mPFC of PSD mice. These impairments have also been demonstrated in depressed mice, and both theta- and gamma-oscillation activities functioned as an important role in mental disorders [66–68]. For FLX acts as a regulator of the 5-HT system, the above results made us hypothesize that the EA-mediated effect was associated with the 5-HT, and this hypothesis has been validated by that EA showed a relief of impairment of 5-HT in mPFC or serum, and its efficacy was dependent on the intact function of DRN. In addition, previous reports have pointed out that EA can be an antidepressant achieved by enhancing 5-HT synthesis, upregulating 5-HT1A receptor levels, and increasing 5-HT content in the brain and synaptic gap [69, 70]. Therefore, the role of EA and FLX was suggested to be comparable, both in terms of efficacy and internal mechanism. However, considering the side effects of FLX administration, acupuncture therapy could be an alternative to this Western medicine treatment, although it still needs to be verified by further large-sample and multi-center clinical data in the future. Noteworthily, the efficacy of acupuncture may be relatively slow, and the treatment time is long, which is a major defect for the urgency of clinical treatment of depression.

This finding broadly supports the work of other studies in this area, demonstrating 5-HT participation in the pathogenesis of depression. 5-HT is an important neuromodulator with unique abilities of neuroplasticity. 5-HT interacts with various receptors involved in multiple signal transduction pathways, including 5-HT interactions with astrocytes and glutamate that may play a role in mood disorders and 5-HT neurotransmission that is involved in the formation of neurobiological networks early in development, among other things [71]. To date, 14 subtypes of 5-HT receptors have been identified. In this study, we have validated the importance of the DRN, but regretfully, we did not explore the related changes of 5-HT receptors located at the mPFC, which is worth investigating in the future.

Moreover, there are also other types of neurons in DRN [72], in addition to the 5-HT neurons, such as dopamine (DA)-, CaMKIIα-, and PV-positive neurons [73]. The DA neurons in the DRN were also suggested to be involved in regulating depression-related behaviors [74]; PV-positive neurons showed bidirectional changes during despair-like behavior [39]. In this study, we mainly focused on the role of the 5-HT system and found that the calcium signaling in CaMKIIα or GABA neurons in mPFC was structurally and functionally modulated by TPH2 neurons in the DRN (Fig. 5B, J, K). Besides that, combined with our mRNA sequencing results, in addition to the serotonin system, long-term depression, dopaminergic synapse, GABAergic synapse, and Glutamatergic synapse may all be influencing factors (Fig. 4A–C). These signaling pathways that are significantly altered in the PSD provide new ideas for our future research.

In conclusion, our findings provide strong support for acupuncture treatment having an important modulation of the 5-HT functions participating in the improvements of PSD. Since 5-HT is involved in a wide range of nervous system functions, we suggested that acupuncture might be used as an effective therapeutic intervention to ameliorate related mental disorders.

DATA AVAILABILITY

The data that support the findings of this study are available by reasonable request.

REFERENCES

1. Guo J, Wang J, Sun W, Liu X. The advances of post-stroke depression: 2021 update. J Neurol. 2022;269:1236–49.
2. Yang Z, Zhao Y, Wang Y, Liu X, Jiang Y, Jiang Y, et al. Echinacoside ameliorates post-stroke depression by activating BDNF signaling through modulation of Nrf2 acetylation. Phytomedicine. 2024;128:155433.
3. Cai W, Mueller C, Li YJ, Shen WD, Stewart R. Post stroke depression and risk of stroke recurrence and mortality: a systematic review and meta-analysis. Ageing Res Rev. 2019;50:102–9.
4. Zhou H, Wei YJ, Xie GY. Research progress on post-stroke depression. Exp Neurol. 2024;373:114660.
5. Zhou J, Fangma Y, Chen Z, Zheng Y. Post-stroke neuropsychiatric complications: types, pathogenesis, and therapeutic intervention. Aging Dis. 2023;14:2127–52.
6. Le JJ, Yi T, Qi L, Li J, Shao L, Dong JC. Electroacupuncture regulate hypothalamic-pituitary-adrenal axis and enhance hippocampal serotonin system in a rat model of depression. Neurosci Lett. 2016;615:66–71.

7. Harmer CJ. Serotonin and emotional processing: does it help explain antidepressant drug action? Neuropharmacology. 2008;55:1023–8.
8. Frank D, Gruenbaum BF, Zlotnik A, Semyonov M, Frenkel A, Boyko M. Pathophysiology and current drug treatments for post-stroke depression: a review. Int J Mol Sci. 2022;23:15114.
9. Li C, Xu X, Wang Z, Wang Y, Luo L, Cheng J, et al. Exercise ameliorates post-stroke depression by inhibiting PTEN elevation-mediated upregulation of TLR4/NF-κB/NLRP3 signaling in mice. Brain Res. 2020;1736:146777.
10. Birch S, Robinson N. Acupuncture as a post-stroke treatment option: A narrative review of clinical guideline recommendations. Phytomedicine. 2022;104:154297.
11. Liu R, Zhang K, Tong QY, Cui GW, Ma W, Shen WD. Acupuncture for post-stroke depression: a systematic review and meta-analysis. BMC Complement Med Ther. 2021;21:109.
12. Lam Ching W, Li HJ, Guo J, Yao L, Chau J, Lo S, et al. Acupuncture for post-stroke depression: a systematic review and network meta-analysis. BMC Psychiatry. 2023;23:314.
13. Zhang K, Cui G, Gao Y, Shen W. Does acupuncture combined with antidepressants have a better therapeutic effect on post-stroke depression? A systematic review and meta-analysis. Acupunct Med. 2021;39:432–40.
14. Wang X, Xiong J, Yang J, Yuan T, Jiang Y, Zhou X, et al. Meta-analysis of the clinical effectiveness of combined acupuncture and Western Medicine to treat post-stroke depression. J Tradit Chin Med. 2021;41:6–16.
15. Sachs BD, Ni JR, Caron MG. Brain 5-HT deficiency increases stress vulnerability and impairs antidepressant responses following psychosocial stress. Proc Natl Acad Sci USA. 2015;112:2557–62.
16. Nikisch G, Mathé AA, Czernik A, Eap CB, Jiménez-Vasquez P, Brawand-Amey M, et al. Stereoselective metabolism of citalopram in plasma and cerebrospinal fluid of depressive patients: relationship with 5-HIAA in CSF and clinical response. J Clin Psychopharmacol. 2004;24:283–90.
17. Villa RF, Ferrari F, Moretti A. Post-stroke depression: mechanisms and pharmacological treatment. Pharmacol Ther. 2018;184:131–44.
18. Han X, Gao Y, Yin X, Zhang Z, Lao L, Chen Q, et al. The mechanism of electroacupuncture for depression on basic research: a systematic review. Chin Med. 2021;16:10.
19. Shin HK, Lee SW, Choi BT. Modulation of neurogenesis via neurotrophic factors in acupuncture treatments for neurological diseases. Biochem Pharmacol. 2017;141:132–42.
20. Yu H, Cao X, Li W, Liu P, Zhao Y, Song L, et al. Targeting connexin 43 provides anti-inflammatory effects after intracerebral hemorrhage injury by regulating YAP signaling. J Neuroinflammation. 2020;17:322.
21. Vahid-Ansari F, Lagace DC, Albert PR. Persistent post-stroke depression in mice following unilateral medial prefrontal cortical stroke. Transl Psychiatry. 2016;6:e863.
22. Shen EY, Chen FJ, Chen YY, Lin MF. Locating the acupoint baihui (GV20) beneath the cerebral cortex with MRI reconstructed 3D neuroimages. Evid Based Complement Alternat Med. 2011;2011:362494.
23. Yuan S, Qiu B, Liang Y, Deng B, Xu J, Tang X, et al. Role of TRPV1 in electroacupuncture-mediated signal to the primary sensory cortex during regulation of the swallowing function. CNS Neurosci Ther. 2024;30:e14457.
24. Wu J, Hua L, Liu W, Yang X, Tang X, Yuan S, et al. Electroacupuncture exerts analgesic effects by restoring hyperactivity via cannabinoid type 1 receptors in the anterior cingulate cortex in chronic inflammatory pain. Mol Neurobiol. 2024;61:2949–63.
25. Ju X, Wang S, Yan P, Zhu C, Hu X, Dong J, et al. Rapid eye movement sleep deprivation combined with fluoxetine protects against depression-induced damage and apoptosis in rat hippocampi via A1 adenosine receptor. Front Psychiatry. 2021;12:599399.
26. Cui S, Yao S, Wu C, Yao L, Huang P, Chen Y, et al. Electroacupuncture involved in motor cortex and hypoglossal neural control to improve voluntary swallowing of poststroke dysphagia mice. Neural Plast. 2020;2020:8857543.
27. Huang J, Huang W, Yi J, Deng Y, Li R, Chen J, et al. Mesenchymal stromal cells alleviate depressive and anxiety-like behaviors via a lung vagal-to-brain axis in male mice. Nat Commun. 2023;14:7406.
28. Li YD, Luo YJ, Chen ZK, Quintanilla L, Cherasse Y, Zhang L, et al. Hypothalamic modulation of adult hippocampal neurogenesis in mice confers activity-dependent regulation of memory and anxiety-like behavior. Nat Neurosci. 2022;25:630–45.
29. Tan T, Wang W, Liu T, Zhong P, Conrow-Graham M, Tian X, et al. Neural circuits and activity dynamics underlying sex-specific effects of chronic social isolation stress. Cell Rep. 2021;34:108874.
30. Qian LX, Jiang YT, Lin FC. Mechanism of the acupoints of the governor vessel in treatment of post-stroke depression on the base of the specificity of meridian points. World J Acupunct-Moxibust. 2019;29:244–8.
31. Duan G, He Q, Pang Y, Chen W, Liao H, Liu H, et al. Altered amygdala resting-state functional connectivity following acupuncture stimulation at BaiHui (GV20) in first-episode drug-Naïve major depressive disorder. Brain Imaging Behav. 2020;14:2269–80.
32. Pracucci E, Graham RT, Alberio L, Nardi G, Cozzolino O, Pillai V, et al. Daily rhythm in cortical chloride homeostasis underpins functional changes in visual cortex excitability. Nat Commun. 2023;14:7108.
33. Hu YT, Tan ZL, Hirjak D, Northoff G. Brain-wide changes in excitation-inhibition balance of major depressive disorder: a systematic review of topographic patterns of GABA- and glutamatergic alterations. Mol Psychiatry. 2023;28:3257–66.
34. Duman RS, Sanacora G, Krystal JH. Altered Connectivity in Depression: GABA and Glutamate Neurotransmitter Deficits and Reversal by Novel Treatments. Neuron. 2019;102:75–90.
35. Yin YY, Yan JZ, Lai SX, Wei QQ, Sun SR, Zhang LM, et al. Gamma oscillations in the mPFC: A potential predictive biomarker of depression and antidepressant effects. Prog Neuropsychopharmacol Biol Psychiatry. 2024;129:110893.
36. Fitzgerald PJ, Watson BO. Gamma oscillations as a biomarker for major depression: an emerging topic. Transl Psychiatry. 2018;8:177.
37. Nyström C, Matousek M, Hällström T. Relationships between EEG and clinical characteristics in major depressive disorder. Acta Psychiatr Scand. 1986;73:390–4.
38. Seo C, Guru A, Jin M, Ito B, Sleezer BJ, Ho YY, et al. Intense threat switches dorsal raphe serotonin neurons to a paradoxical operational mode. Science. 2019;363:538–42.
39. Zhou L, Liu D, Xie Z, Deng D, Shi G, Zhao J, et al. Electrophysiological characteristics of dorsal raphe nucleus in tail suspension test. Front Behav Neurosci. 2022;16:893465.
40. Paquelet GE, Carrion K, Lacefield CO, Zhou P, Hen R, Miller BR. Single-cell activity and network properties of dorsal raphe nucleus serotonin neurons during emotionally salient behaviors. Neuron. 2022;110:2664–79.e8.
41. Jacobs BL, Azmitia EC. Structure and function of the brain serotonin system. Physiol Rev. 1992;72:165–229.
42. Ma J, Wang R, Chen Y, Wang Z, Dong Y. 5-HT attenuates chronic stress-induced cognitive impairment in mice through intestinal flora disruption. J Neuroinflammation. 2023;20:23.
43. Yao LL, Yuan S, Wu ZN, Luo JY, Tang XR, Tang CZ, et al. Contralateral S1 function is involved in electroacupuncture treatment-mediated recovery after focal unilateral M1 infarction. Neural Regen Res. 2022;17:1310–7.
44. Hackett ML, Pickles K. Part I: frequency of depression after stroke: an updated systematic review and meta-analysis of observational studies. Int J Stroke. 2014;9:1017–25.
45. Towfighi A, Ovbiagele B, El Husseini N, Hackett ML, Jorge RE, Kissela BM, et al. Poststroke depression: a scientific statement for healthcare professionals from the American Heart Association/American Stroke Association. Stroke. 2017;48:e30–e43.
46. Wan Y, Holste KG, Hua Y, Keep RF, Xi G. Brain edema formation and therapy after intracerebral hemorrhage. Neurobiol Dis. 2023;176:105948.
47. Keins S, Abramson JR, Mallick A, Castello JP, Rodriguez-Torres A, Popescu D, et al. Association of depression onset and treatment with blood pressure control after intracerebral hemorrhage. Stroke. 2023;54:105–12.
48. Jensen MP, Ziff OJ, Banerjee G, Ambler G, Werring DJ. The impact of selective serotonin reuptake inhibitors on the risk of intracranial haemorrhage: A systematic review and meta-analysis. Eur Stroke J. 2019;4:144–52.
49. Kubiszewski P, Sugita L, Kourkoulis C, DiPucchio Z, Schwab K, Anderson CD, et al. Association of selective serotonin reuptake inhibitor use after intracerebral hemorrhage with hemorrhage recurrence and depression severity. JAMA Neurol. 2020;78:1–8.
50. Akoudad S, Aarts N, Noordam R, Ikram MA, Tiemeier H, Hofman A, et al. Antidepressant use is associated with an increased risk of developing microbleeds. Stroke. 2016;47:251–4.
51. Zhao A, Ma B, Xu L, Yao M, Zhang Y, Xue B, et al. Jiedu Tongluo Granules Ameliorates post-stroke depression rat model via regulating NMDAR/BDNF signaling pathway. Front Pharmacol. 2021;12:662003.
52. Qinlin F, Qi X, Qiong C, Lexing X, Peixia S, Linlin H, et al. Differential expression analysis of microRNAs and mRNAs in the mouse hippocampus of post-stroke depression (PSD) based on transcriptome sequencing. Bioengineered. 2022;13:3582–96.
53. Ifergane G, Boyko M, Frank D, Shiyntum HN, Grinshpun J, Kuts R, et al. Biological and behavioral patterns of post-stroke depression in rats. Can J Neurol Sci. 2018;45:451–61.
54. Han K, Liu J, Tang Z, Su W, Liu Y, Lu H, et al. Effects of excitatory transcranial magnetic stimulation over the different cerebral hemispheres dorsolateral prefrontal cortex for post-stroke cognitive impairment: a systematic review and meta-analysis. Front Neurosci. 2023;17:1102311.
55. Klingbeil J, Brandt ML, Stockert A, Baum P, Hoffmann KT, Saur D, et al. Associations of lesion location, structural disconnection, and functional diaschisis with depressive symptoms post stroke. Front Neurol. 2023;14:1144228.

56. Yin YY, Wang YH, Liu WG, Yao JQ, Yuan J, Li ZH, et al. The role of the excitation:inhibition functional balance in the mPFC in the onset of antidepressants. Neuropharmacology. 2021;191:108573.
57. Price JL, Drevets WC. Neural circuits underlying the pathophysiology of mood disorders. Trends Cogn Sci. 2012;16:61–71.
58. Terroni L, Amaro E, Iosifescu DV, Tinone G, Sato JR, Leite CC, et al. Stroke lesion in cortical neural circuits and post-stroke incidence of major depressive episode: a 4-month prospective study. World J Biol Psychiatry. 2011;12:539–48.
59. Kirkman MA, Allan SM, Parry-Jones AR. Experimental intracerebral hemorrhage: avoiding pitfalls in translational research. J Cereb Blood Flow Metab. 2011;31:2135–51.
60. Rosenberg GA, Mun-Bryce S, Wesley M, Kornfeld M. Collagenase-induced intracerebral hemorrhage in rats. Stroke. 1990;21:801–7.
61. Schlunk F, Greenberg SM. The pathophysiology of intracerebral hemorrhage formation and expansion. Transl Stroke Res. 2015;6:257–63.
62. Zhu W, Gao Y, Wan J, Lan X, Han X, Zhu S, et al. Changes in motor function, cognition, and emotion-related behavior after right hemispheric intracerebral hemorrhage in various brain regions of mouse. Brain Behav Immun. 2018; 69:568–81.
63. Okaty BW, Commons KG, Dymecki SM. Embracing diversity in the 5-HT neuronal system. Nat Rev Neurosci. 2019;20:397–424.
64. Yamada M, Kawahara Y, Kaneko F, Kishikawa Y, Sotogaku N, Poppinga WJ, et al. Upregulation of the dorsal raphe nucleus-prefrontal cortex serotonin system by chronic treatment with escitalopram in hyposerotonergic Wistar-Kyoto rats. Neuropharmacology. 2013;72:169–78.
65. Warden MR, Selimbeyoglu A, Mirzabekov JJ, Lo M, Thompson KR, Kim SY, et al. A prefrontal cortex-brainstem neuronal projection that controls response to behavioural challenge. Nature. 2012;492:428–32.
66. Zhang W, Xiong B, Wu Y, Xiao L, Wang W. Local field potentials in major depressive and obsessive-compulsive disorder: a frequency-based review. Front Psychiatry. 2023;14:1080260.
67. Okonogi T, Sasaki T. Theta-Range oscillations in stress-induced mental disorders as an oscillotherapeutic target. Front Behav Neurosci. 2021;15:698753.
68. Yin YY, Lai ZK, Yan JZ, Wei QQ, Wang B, Zhang LM, et al. The interaction between social hierarchy and depression/anxiety: Involvement of glutamatergic pyramidal neurons in the medial prefrontal cortex (mPFC). Neurobiol Stress. 2023;24:100536.
69. Han X, Wu H, Yin P, Chen Z, Cao X, Duan Y, et al. Electroacupuncture restores hippocampal synaptic plasticity via modulation of 5-HT receptors in a rat model of depression. Brain Res Bull. 2018;139:256–62.
70. Muzio L, Brambilla V, Calcaterra L, D'Adamo P, Martino G, Benedetti F. Increased neuroplasticity and hippocampal microglia activation in a mice model of rapid antidepressant treatment. Behav Brain Res. 2016;311:392–402.
71. Di Giovanni G, De Deurwaerdère P. Serotonin research: Crossing scales and boundaries. Neuropharmacology. 2020;181:108340.
72. He Y, Cai X, Liu H, Conde KM, Xu P, Li Y, et al. 5-HT recruits distinct neurocircuits to inhibit hunger-driven and non-hunger-driven feeding. Mol Psychiatry. 2021;26:7211–24.
73. Li Y, Zhong W, Wang D, Feng Q, Liu Z, Zhou J, et al. Serotonin neurons in the dorsal raphe nucleus encode reward signals. Nat Commun. 2016;7:10503.
74. Wang W, Wang D, Zhao D, Xu L, Jiang S, Zhang Y, et al. Dorsal raphe dopaminergic neurons target CaMKII(+) neurons in dorsal bed nucleus of the stria terminalis for mediating depression-related behaviors. Transl Psychiatry. 2024;14:408.

AUTHOR CONTRIBUTIONS

LY and NX designed the experiments. BD, WD, H.Long, and QH completed all the experiments. ZJ, TN, JG, KH, and H.Li for statistical processing of data. LY, DB, WD, and SC wrote the manuscript. The manuscript with revisions was approved by all authors.

FUNDING

This work was supported by the grants from Natural Science Foundation of Guangdong Province of China (2024A1515012282), National Natural Science Foundation of China (82474623), Outstanding Youth Project of the Natural Science Foundation of Guangdong Province (2025B1515020062), Capacity Enhancement Program for First-Level Disciplines of Guangzhou University of Chinese Medicine (GZY2025GB0206), and Guangzhou University of Chinese Medicine Joint University-Institute Science and High-level Hospital Co-construction Project of Technology Innovation Fund-Shenzhen Hospital (GZYFT2024Y09).

COMPETING INTERESTS

The authors declare no competing interests.

ADDITIONAL INFORMATION

Supplementary information The online version contains supplementary material available at https://doi.org/10.1038/s41398-025-03621-y.

Correspondence and requests for materials should be addressed to Lulu Yao.